Phase interrogation surface plasmon resonance hyperspectral imaging sensor for multi-channel high-throughput detection

RUIBIAO MIYAN,[1] **XUELIANG WANG,**[1] **JIE ZHOU,**[1] **YOUJUN ZENG,**[1] **JUNLE QU,**[1] **HO-PUI HO,**[2] **KAIMING ZHOU,**[3] **BRUCE ZHI GAO,**[4] **JIAJIE CHEN,**[1,5] [iD] **AND YONGHONG SHAO**[1,6] [iD]

[1]*College of Physics and Optoelectronics Engineering, Key Laboratory of Optoelectronic Devices and Systems of Ministry of Education and Guangdong Province, Shenzhen University, Shenzhen 518060, China*
[2]*Department of Biomedical Engineering, The Chinese University of Hong Kong, Shatin, Hong Kong*
[3]*Aston Institute of Photonic Technologies, Aston University, Birmingham B4 7ET, United Kingdom*
[4]*Department of Bioengineering and COMSET, Clemson University, Clemson, SC 29634, USA*
[5]*cjj@szu.edu.cn*
[6]*shaoyh@szu.edu.cn*

Abstract: Phase interrogation surface plasmon resonance (SPR) imaging is, in principle, suitable in multiple samples and high-throughput detection, but the refractive index difference of various samples can be largely varied, while the dynamic range of phase interrogation SPR is narrow. So it is difficult to perform multi-sample detection in phase interrogation mode. In this paper, we successfully designed a multi-channel phase interrogation detection SPR imaging sensing scheme based on a common optical interference path between p- and s-polarized light without using any mechanical moving components. The fixed optical path difference between p- and s-polarized light is introduced by a birefringence crystal to produce sinusoidal spectral interference fringes. We adopted a time-division-multiplexing peak-finding algorithm to track the resonance wavelength so that the detection range can cover every channel. The phase values which carry the high sensitivity signal of the corresponding samples are calculated by the iterative parameter scanning cross-correlation algorithm.

1.   Introduction

Surface plasmon resonance (SPR) sensing has the advantages of including high sensitivity and label-free real-time high-throughput detection of biomolecular interactions. SPR has been widely used in environmental monitoring, food safety, medical diagnosis, genomics and proteomics research [1–3]. The latest development direction of SPR technology is to achieve higher throughput and sensitivity with wider detection dynamic range. Notably, the SPR imaging (SPRi) methods are a common approach to realize the high-throughput bio-detection and real-time monitoring [4]. Currently, there are mainly four types of SPR interrogation methods, i.e., intensity interrogation, angular interrogation, spectral interrogation and phase interrogation [5–7]. Among them, the phase interrogation mode offers the most efficient way to enhance the SPR detection sensitivity [8,9], which normally realizes by the interference of p- and s-polarized light components. The interference information is either extracted from spatial domain of two-dimensional (2D) image of fringes [10,11], or time-varying light intensity monitoring from time domain [12]. However, although these techniques can realize SPR phase imaging detection, the incident angle and wavelength of excitation light are generally fixed, so the dynamic range is quite narrow [13–15]. Thus, it becomes difficult to conduct the simultaneous detection of samples with larger refractive index differences in multiple microfluidic channels. Although one can adopt multi-angle incident mode to select best incident angle for different

channels for phase interrogation [16,17], the different incident angles will induce different degrees of imaging distortion, so it is also not suitable for real-time multi-channel SPR imaging detection. Nevertheless, some optical heterodyne methods are suitable for simultaneous detection in phase interrogation by using broader spectrum incidence, so that SPR wavelength for multiple samples can be detected simultaneously [18]. For example, H. P. Ho's group developed a phase interrogation SPR technology based on white-light spectral interferometry by adopting the Michelson\Mach-Zehnder interferometer style, where the SPR phase shift is extracted from the interference components of p- and s- polarized light [19–21]. Although these technologies can flexibly select the best excitation wavelength for samples with large variation, they lack SPR imaging ability. In addition, the common light path based phase interrogation SPR sensing system with birefringence crystal replace modulator (such as LCM [22,23], PEM [24]) or without modulator [25] can also produce sinusoidal spectral interference fringes, in which one can extract the phase information at the optimal excitation wavelength. It not only improves the stability, but also reduces the cost of the system. However, in these schemes, spectrometers are used as the signal detection device which also makes the system unable to conduct SPR imaging and realize simultaneous detection of multiple samples in different channels. To improve the detection throughput of phase interrogation SPR sensors with no electronically controlled modulators, herein, we developed a phase interrogation SPR sensor based on common optical path, which can perform multi-channel SPR hyperspectral imaging. We used halogen lamp as the white light source and acoustic-optic tunable filter (AOTF) to modulate the incident wavelength. The demodulation method of the spectrometer is replaced by the wavelength-scanned imaging method. In addition, we propose a time division multiplexing peak-finding algorithm to find the resonance wavelengths of different samples. At the same time, based on the modulated light signal, the phase shift at resonance condition is calculated by iterative parameter scanning cross-correlation (IPSCC) method [25], and higher sensitivity with wider detection range across different channels for multi-sample detection in phase interrogation mode can be achieved. Comparing with the traditional polynomial fitting method, this method has obvious advantages in detection efficiency, and can simultaneously detect and image multiple channels. In addition, we also did some biological experiments of antibody-antigen to verify the feasibility of the method. The system has shown great noise suppression ability because of the usage of mechanical movement free optical structure and common optical path of s- and p- polarization.

2. Experimental setup

The phase interrogation SPR imaging system is shown in Fig. 1. The p- and s-polarized light components share the same optical path so that the instability induced by other environmental factors is reduced. The 100W halogen lamp (GCI-060101, Daheng, China) is used as the excitation white light source and the white light passes through the liquid core fiber first. Then it is scanned by the AOTF (AOTFnC-VIS-TN, Opto-electronic, France), different wavelengths are selected successively from 600 nm to 680 nm in one scanning cycle. After the scanning light is collimated and expanded, it passes through the polarizer and the special wave plate WP. The polarization direction is 45° corresponding to the optical axis. The wave plate makes the p- and s-polarized light components produce a fixed phase difference. P2 is the analyzer that causes two optical components to interfere with each other in a direction perpendicular to P1. In addition, the sensor module adopted in our system is a commonly used Kretschmann prism SPR sensing structure, which consists of a prism, gold film glass substrate, and flow cell. The prism is made by SF11 glass (refractive index: 1.785 RIU), the thickness of the gold film coated on the glass substrate is 48 nm. SPR phenomenon occurs at the surface of the gold film after excited by the modulated incident light. After the reflected light passes through the sensing surface (gold film), the sample's information is loaded on the light. Subsequently, each pixel of CMOS (DMK37AUX287, Imaging Source, Germany) collects the intensity value of its corresponding

position on the sensing surface. When the system is in operation, the CMOS takes the image of the whole sensing surface each time when the AOTF switches one wavelength. After a scan cycle, each pixel of CMOS produces its own SPR interference spectrum, so that a 2D hyperspectral SPR resonance wavelength imaging can be generated. The synchronicity of AOTF and CMOS in our system is control by a home-made program produced by home-made LabVIEW software.
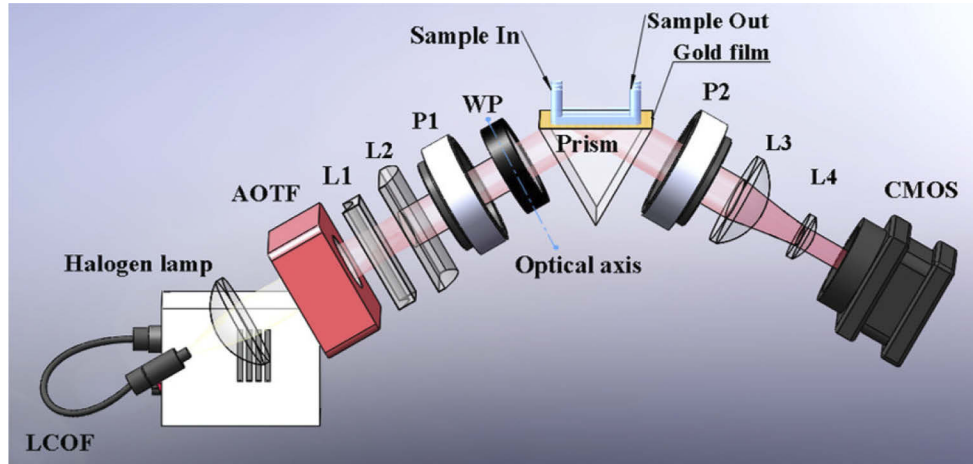

Fig. 1. (a) Schematic of our phase-SPRi biosensor system in Kretschmann configuration. L1-L2, lens; AOTF, Acoustic Optics Tunable Filter; P1 and P2, polarizer; WP, Wave plate, a custom wave plate which can produce an optical path difference of 10^5 nm for its s- and p- component; LCOF, Liquid Core Optical Fiber; CMOS, Complementary Metal-Oxide-Semiconductor.

3. Principle of multi-channel multi-sample detection

3.1. Wavelength scanning

When the excitation light passes through the polarizer P2, the phase difference produced by different wavelengths are different, resulting in different light interference intensity. The formula of interference spectrum is shown as follows:

$$I(\lambda) = I_0(\lambda)\{1 + V_{SPR}(\lambda)\cos[\phi_{OPD} + \phi_{SPR}(\lambda)]\} + I_{Noise} \qquad (1)$$

Where $I_0(\lambda)$ is the light source spectrum, $V_{SPR}(\lambda)$ is the interference fringe contrast, ϕ_{OPD} is the additional phase difference between the p- and s-polarization components introduced by the birefringence crystal WP, and $\phi_{OPD}(\lambda) = |\phi_P - \phi_S|$ is the SPR induced phase shift [25]. And Fig. 2(a) shows the typical interference spectrum. When SPR occurs, the relative phase difference between the s-polarization component and the p-polarization component at the resonance wavelength changes dramatically. Therefore, the most sensitive region is in the vicinity of resonance wavelength.

3.2. Finding SPR phase shift

Noted that the SPR phase shifts differently due to changes in refractive index. Generally, the SPR phase changes linearly with refractive index (RI) within a narrow range of RI for a fixed excitation wavelength. We can achieve multi-channel multi-sample detection through cascading the adjacent linear ranges by selecting different excitation wavelengths according to the refractive index of the sample.
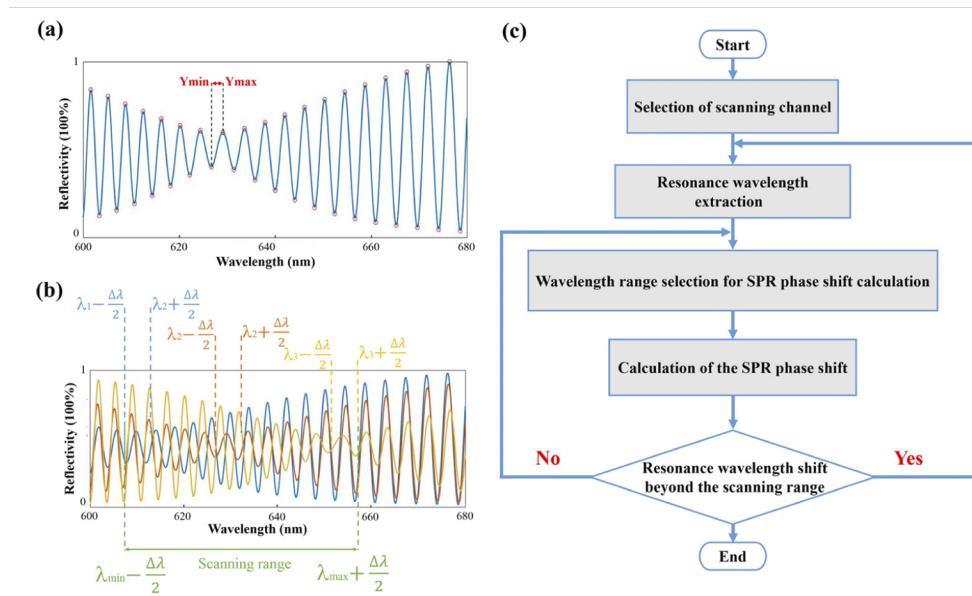
Fig. 2. (a) The SPR interference spectrum with maximum and minimum values marked by peak finding algorithm. (b) The SPR interference spectra of different samples marked in blue, orange, and yellow color. The green line segment represents a smaller scanning wavelength range just in which all the resonant wavelengths are located. (c) Flow chart of wavelength scanning procedure and SPR phase calculation.

To better explain our method, we assume that the three groups of samples experienced the shift in refractive index respectively. As shown in Fig. 2(b), in the spectral region where SPR has occurred, the fringe contrast (peak to peak value) of the interference spectrum will decrease to its lowest value at the resonance wavelength. And there are three steps for extracting the SPR phase:

1) Resonance wavelength extraction. First, an initial scanning of the full spectrum range (600nm-680 nm) on the sensing surface of three microfluidic channels is conducted by AOTF. Then SPR interference spectra of different sensing sites are obtained. As Fig. 2(a) shows, to avoid the uneven distribution of light intensity at each wavelength, the interference spectrum is normalized. Next, we use the peak finding algorithm to find the resonance wavelength: i) We obtain the positions of the peaks and troughs of the interference spectrum via extreme value judgment; ii) Upper envelope and the lower envelope of each spectrum are obtained via interpolation; iii) The minimum value of the upper envelope Y_{min} and the maximum value of the lower envelope Y_{max} of the interference spectrum are obtained respectively, corresponding to the wavelengths of λ_{Ymin} and λ_{Ymax}. Then the resonance wavelength λ is chosen at (λ_{Ymax} +λ_{Ymin})/2. Suppose the corresponding average resonance wavelengths of whole detection points in microfluidic channel 1, 2, and 3 in the Fig. 2(b) are λ_1, λ_2, and λ_3 respectively, where the maximum and the minimum resonance wavelength are λ_{max} and λ_{min}. In order to calculate the phase shift at resonance condition, a complete sinusoidal spectral signal is needed, and the difference between two adjacent peaks has a length of $\Delta\lambda$. Then for the subsequent scanning cycles, in order to shorten the scanning time, instead of full spectrum scanning, a partial wavelength scanning range is set from $\lambda_{min} - \frac{\Delta\lambda}{2}$ to $\lambda_{max} + \frac{\Delta\lambda}{2}$. If the SPR wavelength at each channel is shifted during the scanning, updated λ_1, λ_2, and λ_3 will be obtained respectively and thus will trigger a new scanning range.

2) Wavelength range selection for SPR phase shift calculation. Based on the different initial resonance wavelength of λ_1, λ_2, and λ_3 of channel 1 to 3, we will select different effective

interference spectra for each channel to calculate its phase shift. For example, as the diagram of multi-sample detection working mode in Fig. 2(b) shows, in a partial wavelength scanning range, the effective interference spectrum range used for calculation of each channel is selected as $\lambda_i - \frac{\Delta\lambda}{2}$ to $\lambda_i + \frac{\Delta\lambda}{2}$ (i=1,2,3), which is indicated in blue, orange, and yellow respectively. As the flow chart in Fig. 2(c) illustrated, during the real-time monitoring of the samples flowing through the microfluidic channels, if each channel's resonance wavelength shift is within the partial scanning range($\lambda_{min} - \frac{\Delta\lambda}{2}$ to $\lambda_{max} + \frac{\Delta\lambda}{2}$), then it is repeated to scan at the same range, and the corresponding phase change of different positions can be obtained by analyzing the relevant spectrum.

3) Calculation of the SPR phase shift. The SPR phase is extracted by a new iterative parameter scanning cross-correlation algorithm [25], based on the corresponding phase calculation band ($\lambda_i - \frac{\Delta\lambda}{2}$ to $\lambda_i + \frac{\Delta\lambda}{2}$). In addition, during the real-time detection of multi-channel samples, a time-division-multiplexing method is used. After AOTF scans a phase calculation band (corresponding to a sample), the above resonance wavelength finding process is executed once to find a corresponding resonance wavelength and phase shift, while AOTF continuously scans the next phase calculation band at the same time, the resonance wavelength finding process is repeated again until all the resonant wavelengths and phase shift of multi channels are calculated, the AOTF will start the next partial range scanning cycle. Therefore, this time-division-multiplexing method can make full use of the time-sequence spectrum for multi-channel detections.

4. Results and discussion

The dynamic range is an important parameter for a SPR sensor. For our system, we tested the dynamic range of single channel as well as the detection range across different channels. As shown in Fig. 3, we used three saline water samples with different concentration variation range of 0%-1.2%, 4%-5.2%, and 9%-10.2%, and each sampling point has an increment of 0.2% by volume. And their corresponding refractive index changes are referred from Ref. [26]. During the testing, the incident angle was fixed to 54.5° which is the optimal SPR incident angle for water. The phase shifts of salt solutions in three different channels are shown in Fig. 3. The three channels have the optimal monitoring area respectively, in which their SPR phase shift linearly with the refractive index variation, and each channel's dynamic range is 10^{-4} RIU, which almost reaches the upper limit of the dynamic range of phase interrogation SPR sensor [5,16,17]. However, the three channels can achieve the best excitation wavelength for different samples one after another in temporal sequence, the detection refractive index range across different channels can be as large as 10^{-2} RIU. And this range is mainly limited by the working bandwidth of the SPR system which is mainly determined by the three parameters, i.e., the spectrum range of the excitation light source, the working bandwidth of AOTF, and the FWHM (full width at half maxima) of wave plate. If the working bandwidth of the system is broadened, the detecting range across multiple channels of the system will be further improved.
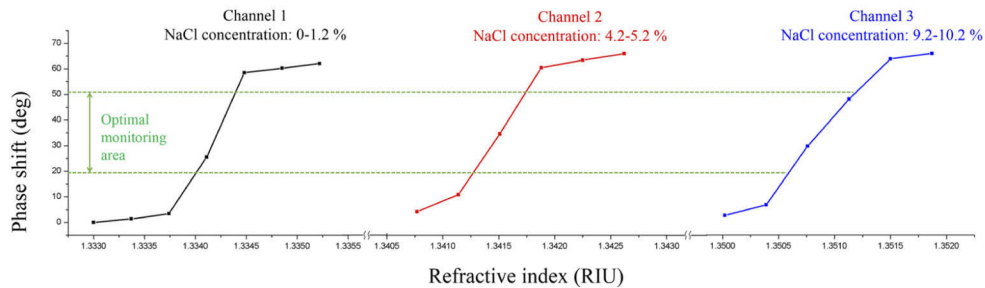

Fig. 3. Phase shift versus refractive index of different channels.

Another important parameter for a sensing system is the sensitivity which can be calculated from formula (2). σ_{RI} is sensitivity, the δn is the refractive index change, the δp is the corresponding shift of resonance phase, and the σ_{SD} is the root mean square (RMS) noise of our system. We inject a deionized water solution into the channel, and continuously detect the phase of the resonance wavelength. We averaged 30×30 pixels for each data point to reduce the noise Therefore, based on the detection noise and the above formula calculation, the sensitivity of the system is 9.1×10^{-7} RIU, which is in the same order as the traditional phase SPR sensor [5,25].

$$\sigma_{RI} = \frac{\delta n}{\delta p} \cdot \sigma_{SD} \tag{2}$$

To assess the capability of our phase sensor for monitoring biomolecular interactions, we performed real-time monitoring of binding interactions between goat anti-human IgG and human IgG antibody. The sensor chip was first rinsed by deionized water, and dried with nitrogen gas, then placed onto the prism, the chip was attached to the coupling prism via a drop of refractive index matching oil. A three-channel flow chamber was used for injecting sample. And the probe fixation process is a typical physical adsorption process: (1) Phosphate buffered saline (PBS, 0.01 M, pH=7.4) was injected into the 3 channels respectively and flushing for 10 min in a flow rate of 10 μl/min, and then the resonance wavelengths of three channels were monitored in real-time; (2) When the resonance wavelengths were stable, human IgG solution (10 μg/ml) was injected into the three channels simultaneously in a flow rate of 10 μl/min, when the human IgG was steadily bonded on the sensing surface of gold film, their resonance wavelengths were stable, then PBS was injected and flushing for 10 min to wash the unbonded human IgG. (3) After the resonance wavelengths were stable, BSA (Bovine Serum Albumin) solution in the concentration of 10 mg/ml was injected into the three channels simultaneously in a flow rate of 10 μl/min. The BSA molecules can occupy the vacancy points without human IgG binding in procedure (1), so as to prevent the nonspecific binding between the sensing surface with the goat anti-human IgG in the next step; (4) Similarly, when the resonance wavelengths were stable, PBS was injected and flushing for 10 min. In the biological binding process, the three channels were injected with PBS, goat anti-human IgG solution in concentrations of 5 μg/ml and 2 μg/ml respectively. The channel with PBS is reference channel, the other two channels are reaction channels. Before the chemical binding, the system conducted wavelength scanning of the sensing surface to find the resonance wavelengths for all channels. Then our SPR system works automatically in the right spectral band. As shown in Fig. 4(a), we obtained the time responsive curve of phase change upon biological sample injection in three channels. The blue curve is the reference channel, the
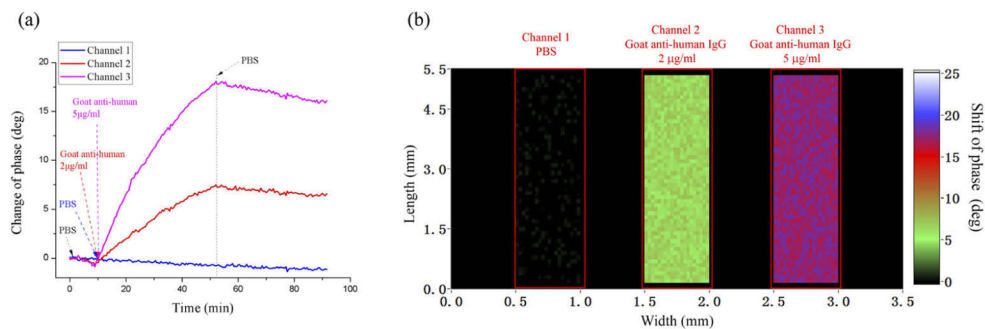

Fig. 4. Measurement of antigen-antibody interaction between Goat anti-human IgG and human IgG. (a)Real-time phase response of antigen–antibody binding reactions, the samples introduced in the three channels from left to right are PBS and 2 μg/ml, and 5 μg/ml human IgG respectively; (b) The image of phase shift at resonance wavelength.

red and pink curves are the reaction channels. The real-time phase detection diagram of the reference channel is unchanged before and after the reaction, while the resonance phase in the reaction channel is significantly different after the reaction, which is induced by the specific binding of antigen and antibody. Moreover, our SPR system also allows us to obtain the phase difference in each pixel before and after the reaction of the sensing surface. As it's illustrated in Fig. 4(b), the color of each pixel in the figure represents the SPR phase difference on the sensing surface before and after the reaction. Therefore, this phase sensor is also favorable for real-time bio-reaction imaging and monitoring.

5. Conclusion

Herein, we have demonstrated a phase sensor for monitoring biomolecular interactions based on a passive phase retarder and time division multiplexing peak finding algorithm, and the scheme is more concise compared with the previous method. The combination of AOTF for incident light wavelength scanning and CMOS for 2D imaging has made our system capable of detecting multiple samples simultaneously and rapidly. In addition, the peak finding algorithm has reduced the number of scanning points per cycle. It has greatly mitigated the time consumption for wavelength selection in scanning devices. Compared with the traditional phase interrogation SPR, the optical path of our system is simpler and has no electrical or mechanical controlled phase modulators. Through the design of multi-concentration saltwater and multi-sample biochemical reaction experiments. The capability to complete the real-time multi-channel biochemical reaction monitoring with high detection efficiency is verified. In terms of future optimization, If the light source with higher light intensity can be used, the noise suppression ability of the system will be further improved. Moreover, the sample species for detection are limited by the excitation spectrum range of the halogen lamp. One can adopt a broader band light source to have more types of samples tested simultaneously. In addition, there is also a sensitivity disparity between the theory and our device which is induced by the spectral bandwidth (4 nm) from the wavelength selecting device AOTF. A high-performance wavelength filter with a narrower bandwidth can further improve the sensitivity.

Disclosures. The authors declare no conflicts of interest.

Data availability. Data underlying the results presented in this paper are not publicly available at this time but can be obtained from the authors upon reasonable request.

References

1. B. Liedberg, I. Lundström, and E. Stenberg, "Principles of biosensing with an extended coupling matrix and surface plasmon resonance," Sens. Actuators, B **11**(1-3), 63–72 (1993).
2. L. Wu, J. Guo, X. Dai, Y. Xiang, and D. Fan, "Sensitivity enhanced by MoS2-graphene hybrid structure in Guided-wave surface plasmon resonance biosensor," Plasmonics **13**(1), 281–285 (2018).
3. Y. Zeng, J. Zhou, X. Wang, Z. Cai, and Y. Shao, "Wavelength-scanning surface plasmon resonance microscopy: A novel tool for real time sensing of cell-substrate interactions," Biosens. Bioelectronics **145** 145, 111717(2019).
4. N. Aldred, T. Ekblad, O. Andersson, B. Liedberg, and A. S. Clare, "Real-time quantification of microscale bioadhesion events in situ using imaging surface plasmon resonance (iSPR)," ACS Appl. Mater. Interfaces **3**(6), 2085–2091 (2011).
5. Y. Zeng, R. Hu, L. Wang, D. Gu, J. N. He, S. Y. Wu, H. P. Ho, X. J. Li, J. L. Qu, B. Z. Gao, and Y. Shao, "Recent advances in surface plasmon resonance imaging: detection speed, sensitivity, and portability," Nanophotonics **6**(5), 1017–1030 (2017).
6. D. Shi, W. Peng, and Y. Xinglong, "Phase-Sensitive Surface Plasmon Resonance Sensors: Recent Progress and Future Prospects," Sensors **17**(12), 2819–2833 (2017).
7. Y. Zeng, X. Wang, S. Y. Wu, J. N. He, J. Qu, X. J. Li, H. P. Ho, D. Y. Gu, B. Z. Gao, and Y. Shao, "High-throughput imaging surface plasmon resonance biosensing based on an adaptive spectral-dip tracking scheme," Opt. Express **24**(25), 28303–28311 (2016).

8. D. V. Sotnikov, A. V. Zherdev, and B. B. Dzantiev, "Detection of intermolecular interactions based on surface plasmon resonance registration," Biochemistry (Moscow) **80**(13), 1820–1832 (2015).
9. Y. H. Huang, H. P. Ho, S. K. Kong, and A. V. Kabashin, "Phase-sensitive surface plasmon resonance biosensors: methodology, instrumentation and applications," Ann. Phys. **524**(11), 637–662 (2012).
10. F. Yang, W. Song, C. Zhang, H. Fang, C. J. Min, and X. C. Yuan, "A Phase-Shifted Surface Plasmon Resonance Sensor for Simultaneous Photoacoustic Volumetric Imaging and Spectroscopic Analysis," ACS Sens. **6**(5), 1840–1848 (2021).
11. B. J. Jayeta, M. H. Bera, and M. Ray, "Split Mach–Zehnder interferometer for surface plasmon resonance based phase modulation," Opt. Commun. **403**, 55–61 (2017).
12. H. K. H. X. C. Du, L. Wang, X. Wang, J. S. Zhu, Y. Gao, B. Peng, H. X. Hao, and N. B. Cai, "Detection of morphine in urine based on a surface plasmon resonance imaging immunoassay," Anal. Methods **12**(23), 3038–3044 (2020).
13. D. Wang, J. F. C. Loo, J. Chen, Y. Yam, S. C. Chen, H. He, S. K. Kong, and H. P. Ho, "Recent advances in surface plasmon resonance imaging sensors," Sensors **19**(6), 1266–1292 (2019).
14. P. Mihaela and B. Camelia, "SPR and SPR Imaging: Recent Trends in Developing Nanodevices for Detection and Real-Time Monitoring of Biomolecular Events," Sensors **16**(6), 870–885 (2016).
15. C. L. Wong and M. Olivo, "Surface Plasmon Resonance Imaging Sensors: A Review," Plasmonics **9**(4), 809–824 (2014).
16. Y. Huang, H. P. Ho, S. Y. Wu, S. K. Kong, W. W. Wong, and P. Shum, "Phase sensitive SPR sensor for wide dynamic range detection," Opt. Express **36**(20), 4092–4093 (2011).
17. G. Q. Lan and Y. C. Gao, "Surface plasmon resonance sensor with high sensitivity and wide dynamic range," IEEE Sens. J. **18**(13), 5329–5333 (2018).
18. Y. Huang, H. P. Ho, S. Y. Wu, and S. K. Kong, "Detecting Phase Shifts in Surface Plasmon Resonance: A Review," Adv. Opt. Technol. **2012**, 1–12 (2012).
19. S. P. Ng, C. M. L. Wu, S. Y. Wu, and H. P. Ho, "White-light spectral interferometry for surface plasmon resonance sensing applications," Opt. Express **19**(5), 4521–4527 (2011).
20. Y. Wang, S. Zeng, A. Crunteanu, Z. Xie, G. Humbert, L. Ma, Y. Wei, A. Brunel, B. Bessette, J.-C. J. N.-m. l. Orlianges, F. Lalloué, O. G. Schmidt, N. Yu, and H.P. Ho, "Targeted Sub-Attomole Cancer Biomarker Detection Based on Phase Singularity 2D Nanomaterial-Enhanced Plasmonic Biosensor," Nano-Micro Lett. **13**(1), 1–11 (2021).
21. S. P. Ng, C. M. L. Wu, S. Y. Wu, H. P. Ho, and S. K. Kong, "Differential spectral phase interferometry for wide dynamic range surface plasmon resonance biosensing," Biosens. Bioelectron. **26**(4), 1593–1598 (2010).
22. Y. Shao, Y. Li, D. Y. Gu, K. Zhang, J. L. Qu, J. N. He, X. J. Li, S. Y. Wu, H. P. Ho, M. G. Somekh, and H. B. Niu, "Wavelength-multiplexing phase-sensitive surface plasmon imaging sensor," Opt. Lett. **38**(9), 1370–1372 (2013).
23. S. P. Ng, F. C. Loo, S. Y. Wu, S. K. Kong, C. M. L. Wu, and H. P. Ho, "Common-path spectral interferometry with temporal carrier for highly sensitive surface plasmon resonance sensing," Opt. Express **21**(17), 20268–20273 (2013).
24. P. P. Markowicz, W. C. Law, A. Baev, P. N. Prasad, and A. V. Kabashin, "Phase-sensitive time-modulated surface plasmon resonance polarimetry for wide dynamic range biosensing," Opt. Express **15**(4), 1745–1754 (2007).
25. Y. Zeng, X. Wang, J. Zhou, R. Miyan, J. L. Qu, H.-P. Ho, K. Zhou, B. Gao, and Y. Shao, "Phase interrogation SPR sensing based on white light polarized interference for wide dynamic detection range," Opt. Express **28**(3), 3442–3450 (2020).
26. W. M. Haynes, *CRC Handbook of Chemistry and Physics*, 95th ed. (CRC, 2014).